ISSN 1819-7140, Russian Journal of Pacific Geology, 2009, Vol. 3, No. 5, pp. 477–490. © Pleiades Publishing, Ltd., 2009.
Original Russian Text © Yu.L. Rebetsky, 2009, published in Tikhookeanskaya Geologiya, 2009, Vol. 28, No. 5, pp. 70–84.

Stress State of the Earth's Crust of the Kuril Islands and Kamchatka before the Simushir Earthquake

Yu. L. Rebetsky

Schmidt Institute of Physics of the Earth, Russian Academy of Sciences, Moscow, Russia

Received January 20, 2009

Abstract—The field of modern tectonic stresses was reconstructed for the Earth's crust of the northwestern segment of the Pacific subduction zones. For this purpose, we used the method of cataclastic analysis and data on the magnitude of the stresses released at the source of the Simushir earthquake of 2006, which allowed us to determine both the orientation of the principal stress axes and the magnitude of the stresses and to estimate the effective strength of rock masses. The effective cohesion was estimated for this region of the Earth's crust as 12 bar, and the maximum shear stresses are no higher than 300 bar. The analysis of the reconstructed stress field in the zone of the preparation of the Simushir earthquake showed that this region was almost free of domains with high stresses where brittle failure requires considerable energy inputs. The medium level of effective pressure indicates that this region is most favorable for the development of a large-scale brittle failure.

Key words: the Earth's crust, tectonic stress, effective strength, brittle failure, earthquake, Kuril Islands, Kamchatka Peninsula.

DOI: 10.1134/S1819714009050108

INTRODUCTION

Since the 1970s, the areas of future strong earthquakes have been predicted by Fedotov [17] for the northwestern flank of the Pacific subduction zones on the basis of distinguishing seismic gaps of the second type. This approach is based on the analysis of the distribution of strong events along a large seismogenic zone and relies in fact on the suggestion that the accumulated elastic strain energy can dissipate only at the expense of strong seismic events. The segment of such a zone in which a strong event has not been observed for a long time is distinguished as most hazardous. In accordance with Fedotov's concept, in the beginning of the 21th century, strong earthquakes with magnitudes of $M > 8$ are to be expected in the southern part of the Kuril arc near Shikotan Island and within the segment between Simushir and Paramushir islands. The area east-northeast of Simushir Island was a source of two strong earthquakes at the end of 2006 and beginning of 2007.

Currently, there are prerequisites for the development of methods of seismic hazard prediction on the basis of new concepts concerning earthquake preparation processes. These methods should rely on new approaches to the reconstruction of natural stresses [15] and the analysis of the spatial distribution of the stress parameters in the preparation zones of strong earthquakes [14]. Hereafter, we will use the term stress reconstruction to indicate that the stress parameters are obtained by the solution of the inverse problem of tectonophysics [1]. One of the most promising among such new methods of reconstruction is the method of the cataclastic analysis (MCA) of sets of earthquake focal mechanisms [14] allowing the determination of both the orientation and magnitude of the principal stresses. The application of this method to the preparation zone of the catastrophic Sumatra–Andaman earthquake allowed us to distinguish a number of specific features of the stress distribution controlling "favorable conditions" for the formation of an earthquake source [11, 12]. It appeared that the major portion of the seismic energy released during this earthquake was related to the ìrippingî of a segment in the western flank of the Sunda arc occurring in the Coulomb–Mohr limiting state but having the lowest level of isotropic stresses (confining pressure). It was shown that a strong earthquake is initiated from a relatively small (compared with the area favorable for the appearance of a strong earthquake) part of a regional fault with a high level of stress gradient. Areas with elevated stress gradients are metastable zones in the Earth's crust [2].

Taking into account Fedotov's concept of earthquake prediction and the occurrence of earthquakes with magnitudes of $M_w = 8.3$ (November 15, 2006) and $M_w = 8.1$ (January 13, 2007) in the subduction zone near Simushir Island, an important question is whether these earthquakes showed the same regular features in their stress distribution that were detected for the preparation zone of the Sumatra–Andaman earthquake. It should be determined how seismic gaps of the second type are manifested in the stress field.

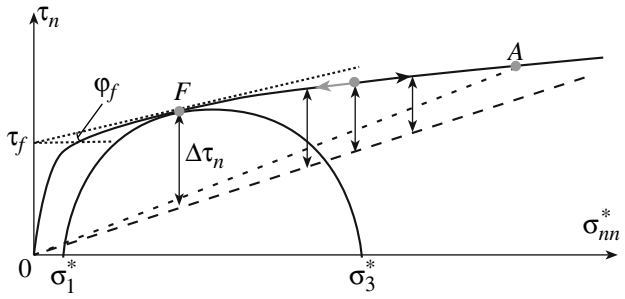

Fig. 1. Relationships of the fields of brittle failure and ductile flow in the Mohr diagram.

The solid curve is the internal strength of rocks; the short- and long-dashed lines are the minimum resistance of dry static friction for the existing fractures and the kinematic friction acting during the relative displacement of their sides; the dotted line corresponds to the determination of strength parameters ($k_f = \tan\gamma_f$ and τ_f) for point F; the vertical segments show the magnitudes of the relaxed stresses for the respective points; the gray and black arrows indicate the directions of the changes in the stress state resulting in more and less efficient brittle failure, respectively.

METHODS OF NATURAL STRESS RECONSTRUCTION

The stress state of the northwestern flank of the Pacific subduction zones was investigated by the MCA of ruptures [6, 25]. This method should be considered as a development of the well-known methods of Carey [21], Gushchenko [3], Gephart [22], and Yunga [18] and the application of some aspects of the theory of plasticity and brittle failure. These aspects of MCA extend the basic concepts of the aforementioned methods and allow one to increase the number of parameters of the stress and seismotectonic strain increment tensors that can be determined. For instance, the previous methods were used to determine the orientation of the major axes of the stress tensor or the seismotectonic strain increment tensor and the coefficient indicating the type of the ellipsoid; the results of the MCA reconstruction may include the full components of the tectonic stress tensor and the normalized components of the seismotectonic strain tensor. The input data for the MCA are seismological evidence on the earthquake focal mechanisms, the magnitude of the stresses relaxed at strong earthquake sources, the topography, and the thicknesses of the major layers of the Earth's crust. The obtained parameters of the stress–strain state are averaged over a scale depending on the magnitude level of the data on earthquake focal mechanisms and the distribution density of seismic events.

The MCA includes several computation stages, and the number of determined parameters of the stress–strain state can be increased depending on the availability of the above data. The first stage includes the determination of the orientation of the principal axes of the stress tensor and the values of the Lode–Nadai coefficient and the selection of such a state from all the possible stress states for which the set of analyzed earthquake focal mechanisms provides the maximum dissipation of the accumulated elastic strain energy [7, 8]. The most important criterion that is used in this method to select in the five-dimensional space (the normal metric space, time, and scale) the earthquake focal mechanisms is the requirement for the elastic strain energy decrease during the earthquake at the desired stress tensor. Together with the maximum principle, this criterion is a consequence of the application of elements of the plasticity theory to a set of rupture deformations.

The selected earthquake sets meeting the above conditions are referred to as homogeneous earthquake samples. They serve to determine the characteristics of the ellipsoids of the stress and seismotectonic strain increment tensors (the principal axes and the type of ellipsoid: uniaxial compression, pure shear, and uniaxial extension) normalized to the slip intensity and characterize the quasi-uniformly deformed area of the Earth's crust (domain) to which the results of stress calculations are assigned. Note that other approaches provide the same set of data but either for the stress tensor [3, 21, 22] or the seismotectonic strain increment tensor [18]. There are no methods, except for MCA, containing algorithms for the simultaneous determination of the parameters of these two tensors.

During the first stage of the MCA, the components of the stress tensor, σ_{ij} (i, j = 1, 2, 3 are the indexes of the coordinate axes of the orthogonal system, for instance, the geographical coordinates), are determined for up to two unknown characteristics of the stress tensor invariant for the choice of the coordinate system: the confining pressure p and the maximum shear stress module τ:

$$\sigma_{ij} = -(p + \tau\mu_\sigma/3)\delta_{ij} + \tau[(1-\mu_\sigma)l_{1i}l_{1j} - (1+\mu_\sigma)l_{3i}l_{3j} + \mu_\sigma\delta_{ij}], \quad \delta_{ii} = 1, \quad \delta_{ij} = 0 \text{ at } i \neq j. \tag{1}$$

where l_{ki} are the direction cosines of the principal axes of the stresses (k = 1, 2, 3) in the selected coordinate system (i), and μ_σ is the Lode–Nadai coefficient ($|\mu_\sigma| \le 1$).

The algorithm employed in MCA for the determination of the p and τ components invokes additional data from studies of the destruction of rock samples [20]. The analysis of these results allows one to distinguish the band of brittle failure in the Mohr diagram, which defines the possible stress states (Fig. 1) both for the newly forming ruptures and for the preexisting reactivated ones [9, 10]. These states are confined between two characteristic curves on the Mohr diagram: the outer failure envelope (strength limit) and the line of the maximum resistance of static friction:

$$\tau_n + k_f\sigma^*_{nn} = \tau_f; \quad \tau_n + k_s\sigma^*_{nn} = 0, \quad \text{at } \sigma^*_{nn} \le 0 \text{ and } \tau_n \ge 0, \tag{2}$$

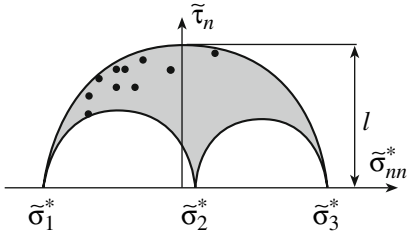

Fig. 2. Reduced Mohr diagram.
The points correspond to the reduced normal and shear stresses acting on a rupture plane at the source of an earthquake from a homogeneous sample.

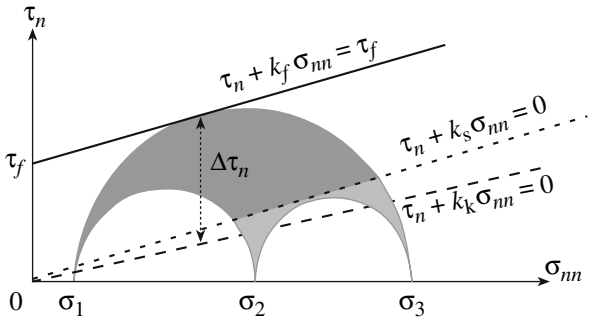

Fig. 3. Reduced Mohr diagram.
The solid line is the approximation of the failure envelope, the short-dashed line is the minimum resistance of static surface friction, the long-dashed line is the resistance of kinematic surface friction, and the vertical segment is the relaxed stresses.

where $k_f(\sigma^*_{nn})$ and $\tau_f(\sigma^*_{nn})$ are the coefficients of the internal friction and the internal cohesion, respectively, which are functions of the effective stress normal to the rupture, σ^*_{nn}, and k is the static surface friction. The left-hand side of Eq. (2) is referred to as the Coulomb stress. Note that the effective normal stress in Eq. (2) accounts for the dependence of the brittle failure on the fluid pressure p_{fl} in the fracture–pore space ($\sigma^*_{nn} = \sigma_{nn} + p_{fl}$) in accordance with the Terzaghi law [16]. Angelier [19] proposed to use the Mohr diagram and the failure field for the estimation of stresses in geologic media.

The stress tensor components obtained after the first stage allow us to calculate the reduced normal and shear stresses, $\tilde{\sigma}_{nn}$ and $\tilde{\tau}_n$, acting on the surface of the rupture generating the earthquake and to project the respective points on the reduced Mohr diagram (Fig. 2), which can be constructed by normalizing the deviatoric components of the stress tensor to τ and subtracting from the normal stresses the value corresponding to the normal stresses (σ_0) on the planes with the maximum shear stresses (τ):

$$\begin{gathered}\sigma_{nn} = \sigma_0 + \tau\tilde{\sigma}_{nn}; \quad \tau_{ns} = \tau\tilde{\tau}_{ns}, \\ \text{at } \sigma_0 = -(p + \tau\mu_\sigma/3), \\ \tilde{\sigma}_{nn} = (1-\mu_\sigma)l^2_{1n} - (1+\mu_\sigma)l^2_{3n} + \mu_\sigma, \\ \tilde{\tau}_{ns} = (1-\mu_\sigma)l_{ni}l_{sj} - (1+\mu_\sigma)l_{3n}l_{3s},\end{gathered} \tag{3}$$

where n is the index of the normal to the nodal plane that acted as the earthquake source, and s is the index of the vector in the rupture plane that defined the direction of the ear stress action.

The Mohr diagram is an efficient tool for the visualization of stressed states and the estimation of their proximity to the limiting state, which corresponds to the transition to either brittle failure or plastic flow (point A in Fig. 1 separates the fields of brittle failure and plastic flow). In the MCA, the failure envelope (Fig. 1) is approximated by a straight line parallel to the line of the static surface friction (Fig. 3). Subsequently, this approximation and the analysis of the scatter on the reduced Mohr diagram of points characterizing the stresses ($\tilde{\sigma}_{nn}$ and $\tilde{\tau}_n$) for the set of earthquakes in each homogeneous sample can be used to determine the normalized values of the maximum shear stresses, τ/τ_f, and the effective confining pressure, p^*/τ_f ($p^* = p - p_{fl}$), up to the unknown value of the effective internal cohesion of the rock mass, τ_f.

The absolute stress values are determined after the estimation of τ_f during the third stage of the reconstruction. This requires additional seismological information on the magnitude of the stresses relaxed at the source of a strong earthquake [11, 12] that occurred in the region. The magnitude of the analyzed earthquake must be higher than the magnitudes of the earthquakes that were previously used to determine the stress tensor components during the first two stages of MCA. It is essential that the characteristic linear size of the source be no smaller than the characteristic linear size defining the scale of the averaging of the stress parameters obtained from the reconstruction. The computational algorithm is based on the possibility to estimate after the first two stages up to the unknown normalizing factor τ_f stresses relaxed along an arbitrarily oriented plane, $\Delta\tau_n$ (Fig. 3):

$$\begin{gathered}\langle\Delta\tau_n/\tau_f\rangle = \tilde{\tau}_n\langle\tau/\tau_f\rangle + k_k(\tilde{\sigma}_{nn}\langle\tau/\tau_f\rangle - \langle\sigma^*_0/\tau_f\rangle), \\ \text{at } \sigma^*_0 = \sigma_0 - p_{fl} \quad \text{and } p^* = p - p_{fl},\end{gathered} \tag{4}$$

where k_k is the coefficient of the kinematic surface friction. The parameters in the angle brackets in the right-hand side of Eq. (4) are determined after the second stage of the reconstruction, and the reduced stresses ($\tilde{\tau}_n$, and $\tilde{\sigma}_{nn}$) are determined after the first stage.

The MCA includes a criterion for distinguishing one of the two nodal planes of the earthquake mechanisms realized as a source. This analysis is based on the calculation of the reduced Coulomb stresses. The selected

realized plane is the nodal plane that is characterized by higher Coulomb stresses:

$$(\tilde{\tau}_n + k_s\tilde{\sigma}_{nn}) - (\tilde{\tau}_s - k_s\tilde{\sigma}_{ss}) > 0, \quad (5)$$

where n and s are the indexes of the normals to the nodal planes of the earthquake focal mechanisms. The analysis of a number of strong events for which the realized plane was determined by geological or seismological methods showed the high reliability of this criterion [15]. There is evidence that this criterion is also applicable for the analysis of weak events [4].

If a strong earthquake occurred in the region for which the first two stages of the MCA stress reconstruction were carried out and the magnitude of the released stresses is known for it from seismological data, the calculation of $\langle\Delta\tau_n/\tau_f\rangle$ for this earthquake using Eq. (4) allows one to estimate the effective strength of the rock mass, τ_f. Given the estimated τ_f value, the absolute values of the maximum shear stresses, τ, and the effective confining pressure, p^*, can be determined.

The calculation of the confining pressure in the rocks (p) requires additional assumptions and additional data. Currently, the MCA invokes the assumption that the normal stresses acting on the horizontal planes are equal to the weight of the overlying rock column. This assumption is often used in geodynamics [27] and requires accounting for the surface topography for the estimation of the average stresses for the crust on the whole (the scale of averaging is a few tens of kilometers) and the relief of the deep crustal layers for averaging over smaller linear scales. Considering the calculation of the average stresses in the crust, the following expression can be written in accordance with the above assumption:

$$p = \gamma h + (\tilde{\sigma}_{zz} - \mu_\sigma/3)\tau, \quad (6)$$

where γ is the density, $h = H_c + H_r$ is the thickness of the rock column from the surface to the depth of the stress reconstruction (H_c is the depth from the zero level for the calculation point, and H_r is the height of the relief from the zero level), and $\tilde{\sigma}_{zz}$ are the reduced vertical stresses (see Eq. (3)). Thus, γh is the weight of the rock column per unit horizontal area determined in the center of the three-dimensional domain whose stress state is reconstructed while accounting for the surface relief averaged with the same averaging window as the data on the stress components. In the case of an oceanic crustal segment, the weight of the water column from the seafloor to the ocean surface must be accounted for in Eq. (6). Previously, Eq. (6) was used within the MCA for the estimation of the confining pressure.

Note that the hypothesis underlying Eq. (6) implies in fact the absence of shear stresses on the vertical and horizontal planes. Such an assumption is a very strong simplification for subduction zones, because the areas of the action of the maximum shear stresses have near-horizontal and near-vertical orientations in these zones [6, 15, 26]. Therefore, in this study, we used, for the first time, a more accurate expression connecting the vertical stresses with the weight of the rocks, which was obtained by the approximation of the crust as a thick plate [15]:

$$p = \gamma h + [(\tilde{\sigma}_{zz} - \mu_\sigma/3)\tau + d(\tilde{\sigma}_{sz}\tau) + d(\tilde{\sigma}_{yz}\tau)]. \quad (7)$$

In this equation, the additional terms compared with Eq. (6) describe the lateral variations in the shear stresses acting on the horizontal planes in two orthogonal directions. After the calculation of the confining pressure, Eq. (4) can be used to determine the fluid pressure in the fracture–pore space of the rocks. The obtained fluid pressures are also average values corresponding to the scale of the averaging of the reconstructed components of the stress tensor. The last procedures of the calculations based on Eq. (7) are in fact equivalent to the introduction of the fourth stage of the MCA for the reconstruction of the stress parameters.

RESULTS OF THE STRESS RECONSTRUCTION

In order to evaluate the characteristic features of the stress state in the preparation areas of strong earthquakes, a regional catalogue of earthquake focal mechanisms was compiled on the basis of the global catalogue of seismological data available on the web site of Harvard University [24]. It includes 1220 earthquakes with magnitudes higher than 4.7 that occurred from 1976 to June 2006 at depths of up to 100 km (Fig. 4). The period of the observations comprises 26 strong earthquakes with magnitudes higher than 7, including the Shikotan earthquake of October 4, 1994 with $M = 8.2$.

The magnitude range of the regional catalogue (Fig. 4) and the density of the earthquake epicenter distribution allowed us to reconstruct the characteristics of the stress state averaging over 30–50 km. Since more than 600 events occurred at depths of more than 30 km and 250 events occurred deeper than 50 km, the stress state parameters were reconstructed in the nodes of a $0.2° \times 0.2°$ grid at depths of 20, 40, and 60 km. All the procedures for the formation of homogeneous samples of earthquake focal mechanisms (first stage of the reconstruction) were accomplished for 778, 835, and 663 quasi-homogeneous domains corresponding to depths of 20, 40, and 60 km; each of the samples contained at least six earthquakes. It should be noted that the grid step was smaller than the characteristic size defining the scale of the stress averaging (50–100 km). Such a step size was selected in order to smooth the spatial variations of the stresses already at this stage of the calculations and to draw the domains analyzed closer to the source of the Simushir earthquake. The data on the relaxed stresses for this earthquake will be used during the further calculations. This paper presents only the results of the reconstruction for the 20 km depth level.

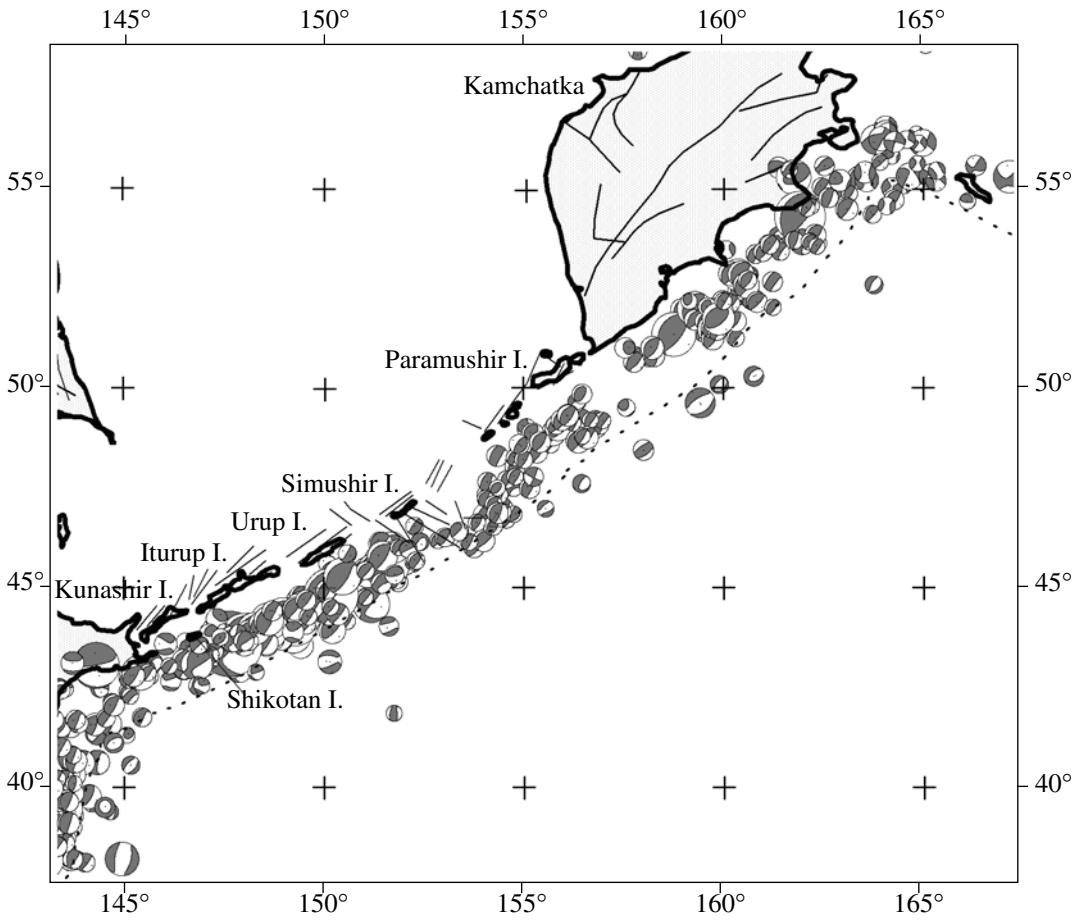

Fig. 4. Focal mechanisms of crustal earthquakes with $M > 5.5$.
The dotted line is the axis of the oceanic trench, and the solid lines are faults.

First Stage of the Stress Reconstruction

The reconstruction of the parameters of the stress ellipsoid and the seismotectonic strain increments performed during the first stage of MCA allowed us to construct maps for the orientation of the principal axes of the stress tensor, the type of the stress tensor, and the characteristics of the stress state. Figure 5 shows the axes of the algebraically maximum and minimum principal stresses constructed in the direction of their plunging and projected onto a horizontal plane for the domains whose centers lie at a depth of 20 km. Note that the results of the reconstruction were thinned for the more convenient graphical presentation.

The axes of the algebraically minimum principle stress σ_3 (Fig. 5a) plunge gently to the southeast (the average strike azimuth is 135°, and the average dip is approximately 19°; Fig. 6a). The dip of these axes decreases toward the island arc and reverses at some points. A rather abrupt change in the σ_3 axis strike was observed at the junction of the Kamchatka segment of the subduction zone with the Aleutian segment. The axes of the algebraically maximum stress, σ_1 (Fig. 5b), plunge steeply toward the back-arc basin. Their average dip is 62° (Fig. 6b). These axes show more considerable deviations from the average strike (290°C) compared with σ_3. Two areas deserve special attention: the junction of the Kamchatka and Aleutian segments of the subduction zones and the southwestern segment near Hokkaido Island, where the orientation of the axes of these stresses changes by more than 45°.

The reconstructed direction of the principal stress axes indicates a gentle dip beneath the oceanic plate for the axis of the maximum compression, a steep dip beneath the subcontinental plate for the axis of the minimum compression, and the orientation of the intermediate principal stress along the oceanic trench lineament. This is typical of the principal stresses in subduction zones [15]. Such a distribution of the principal stress axes corresponds to the prevalent regime of horizontal compression (Fig. 7a). Some deviations from this regime were again observed in the northeastern and southwestern segments of the arc. The former segment contains extended domains with the regime of horizontal slipping under the conditions of additional compression, and the latter segment shows evidence for the slip regime. The slip regime was also detected in the crust

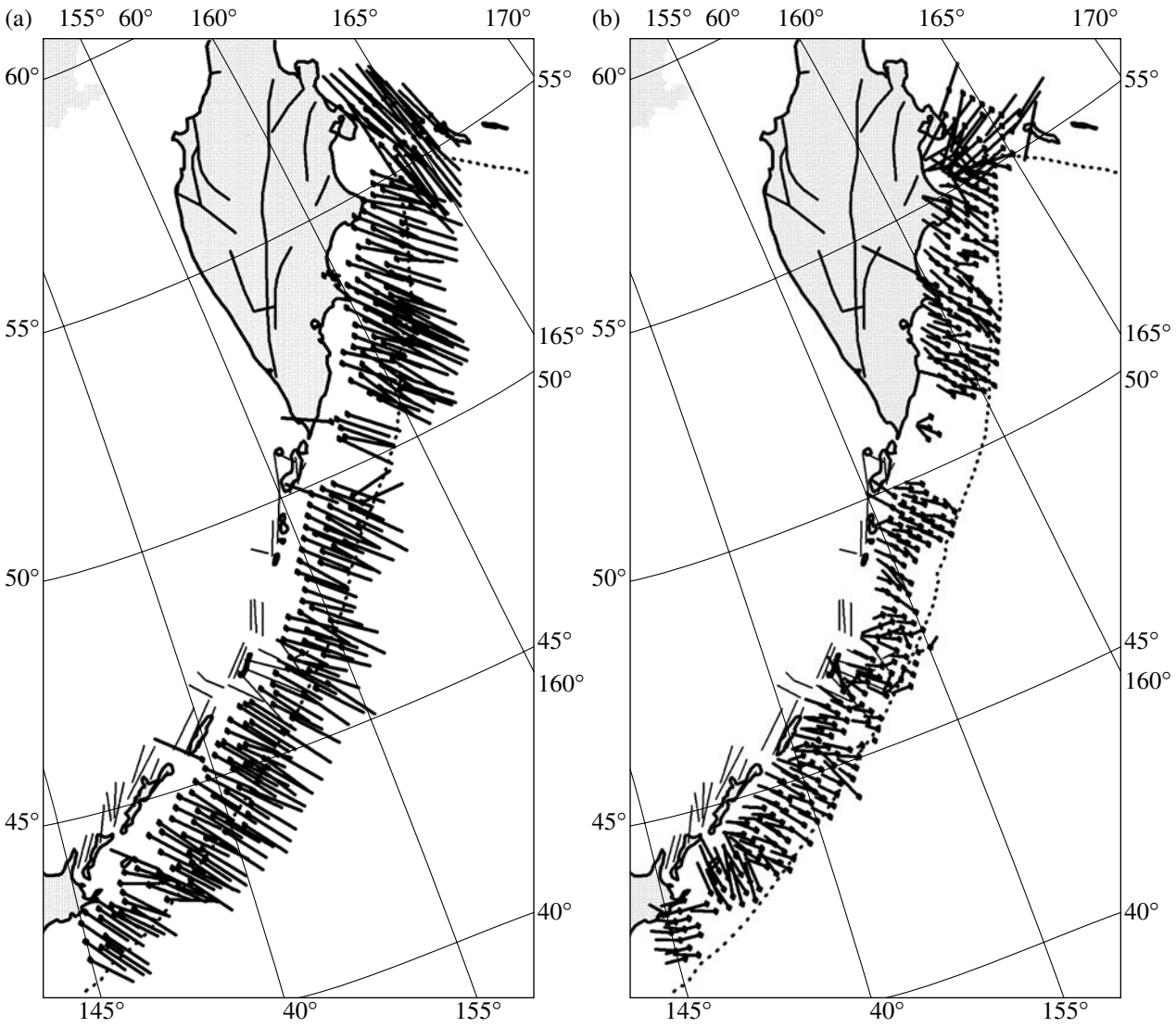

Fig. 5. Projections on the horizontal plane of the axes of plunging of the principal stresses of the maximum deviatoric (a) compression and (b) extension.

along the Kamchatka shore starting from the Shipunsky Peninsula.

The distribution of the stress tensor characteristic defined by the Lode–Nadai coefficient appears to be very homogeneous (Fig. 7b). There is almost everywhere a pure shear tensor, when the algebraically maximum and minimum principal deviatoric stresses are similar in absolute value but opposite in sign (the intermediate principal deviatoric stress is zero). The tensor type (stress ellipsoid) is different in the aforementioned southwestern and northeastern end segments of the region.

The stable orientation of the principal stress axes in the subduction zones is reflected in the stable orientation of the shear stresses acting on the subhorizontal planes (Fig. 8a). Such stresses on the planes whose normals are directed toward the Earth's center indicate the direction of the mantle influence on the crust. In the region considered, these tangential stresses are almost everywhere directed normal to the trench. Such an orientation is consistent with the concept of the convection mechanism of the mantle influence on the moving oceanic lithospheric plate (Fig. 9).

It should be noted that the direction of the action of these stresses is even more stable than the orientation of the axes of the maximum compression, which allows us to consider the shear stresses acting on the subhorizontal planes as an active influence producing the stress state in accordance with the structure of the area considered.

As was noted above, the MCA is unique in that it allows the simultaneous determination of the components of the stress and seismotectonic strain increment tensors. It provides a means of comparing the ellipsoids

of stresses and seismotectonic strain increments using the expression

$$A = \sqrt{(\bar{s}_{ij} - \bar{S}_{ij})(\bar{s}_{ij} - \bar{S}_{ij})}, \quad (8)$$

where $\bar{s}_{ij}$ and $\bar{S}_{ij}$ are the normalized components of the deviators of the stress and seismotectonic strain increment tensors, respectively.

The parameters of Eq. (8) are normalized to the maximum shear stress and the maximum shear strain. If the ellipsoids of stresses and seismotectonic stress increments are similar (their principal axes coincide and the Lode–Nadai coefficients are identical), then $A = 0$, and the medium for which this value was obtained is mechanically isotropic. The maximum differences between these tensors correspond to $A \approx 3$. The values of $A > 0$ define the degree of medium anisotropy.

Based on Eq. (8), we distinguished areas with similar ellipsoids of stresses and seismotectonic strain increments (Fig. 8b). Among such areas are segments near the junction of the Kamchatka and Aleutian subduction zones and near Shikotan Island. The anisotropy of the former segment is probably related to the sharp bend of the subducted lithospheric plate, whereas that of the second segment is probably controlled by the specific features of the deep crustal structure.

Second Stage of the Stress Reconstruction

The homogeneous samples of the earthquake focal mechanisms compiled for each of the 778 domains (depth of 20 km) allowed us to calculate, in accordance with the MCA algorithm, the normalized values of the effective confining pressure, p^*/τ_f (Fig. 10a), and the maximum shear stresses, τ^*/τ_f. The region under investigation showed a rather mosaic distribution of the effective confining pressure (along Iturup and Urup islands and the Kamchatka shore). On the other hand, there are several large areas (150–250 km) where this parameter is relatively stable, and the values from 4 to 12 correspond to its medium level. Such areas were detected near Shikotan, Simushir, and Paramushir islands and near the junction of the Kamchatka and Aleutian subduction zones.

Figure 10b shows the distribution of the ratio of the maximum shear stress to the effective confining pressures, τ/p^*, which ranges in the region from 0.5 to 1.7. The maximum values correspond to the minimum level of the effective confining pressure (Fig. 11). The dark-filled fields in Figs. 10b and 11 correspond to areas showing average or below average levels of the effective confining pressure. In accordance with the concept presented here, these areas are potentially hazardous for complete destruction during the dynamic development of a rupture.

Note that the value $\tau/p^* \approx 0.6$ corresponds to the effective (i.e., corresponding to the scale of averaging) coefficient of the internal friction in the rock mass, k_f,

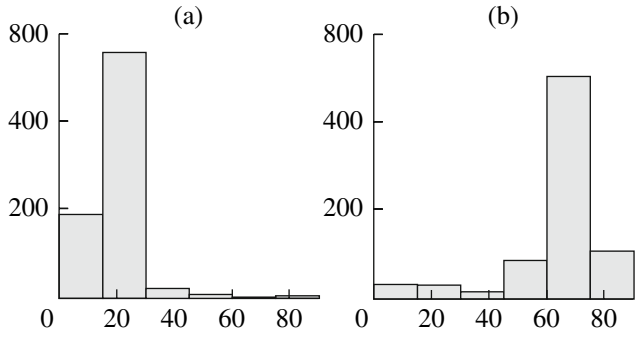

Fig. 6. Diagrams of the dips of the axes of the principal stresses of the maximum deviatoric (a) compression and (b) extension.

accepted during the second stage of the MCA calculations. At higher stress values, the right-hand side of Eq. (2) provides a small contribution to the resistance to the fracture destruction, and the main resistance is generated by the friction forces, $k\sigma_n^*$.

Third Stage of the Stress Reconstruction

The third stage of the reconstruction was based on the use of seismological data on the energy parameters of the first of the two strong Simushir earthquakes. According to the data available on the web site of Harvard University, the energy released in the seismic waves, E_s, and the seismic moment of the earthquake of November 15, 2006, M_0, were 7.4×10^{16} J and 3.4×10^{21} J, respectively. The magnitude of the relaxed stresses can be calculated using the following equation [5]:

$$\Delta\tau_n = 2\mu E_s/M_0. \quad (9)$$

Assuming that the shear modulus is $\mu = 4 \times 10^{10}$ Pa, Eq. (9) yields $\Delta\tau_n = 17 \times 10^5$ Pa.

On the other hand, the magnitude of the relaxed stresses can be estimated up to the normalization to the unknown value of the effective cohesion of the rock mass, τ_f, using the results of the first two stages of the MCA reconstruction and Eq. (6). The analysis of the aftershock zone accounting for the possible geometry of the earthquake source [23] showed that the rupture occurred on one of the nodal planes corresponding to the shallow subduction of the oceanic plate beneath the continental plate. The MCA allows discrimination of the nodal planes into that realized as the source and the fictive one on the basis of the stress state data (3).

Figure 12a shows the reduced Mohr diagram for the stresses corresponding to the onset of the source ripping. It shows the parameters of the stress vectors acting on each of the nodal planes. It can be seen that the shallow nodal plane is very close to the plane of the effective internal friction, whereas the second near-vertical nodal plane lies outside the field of the brittle fail-

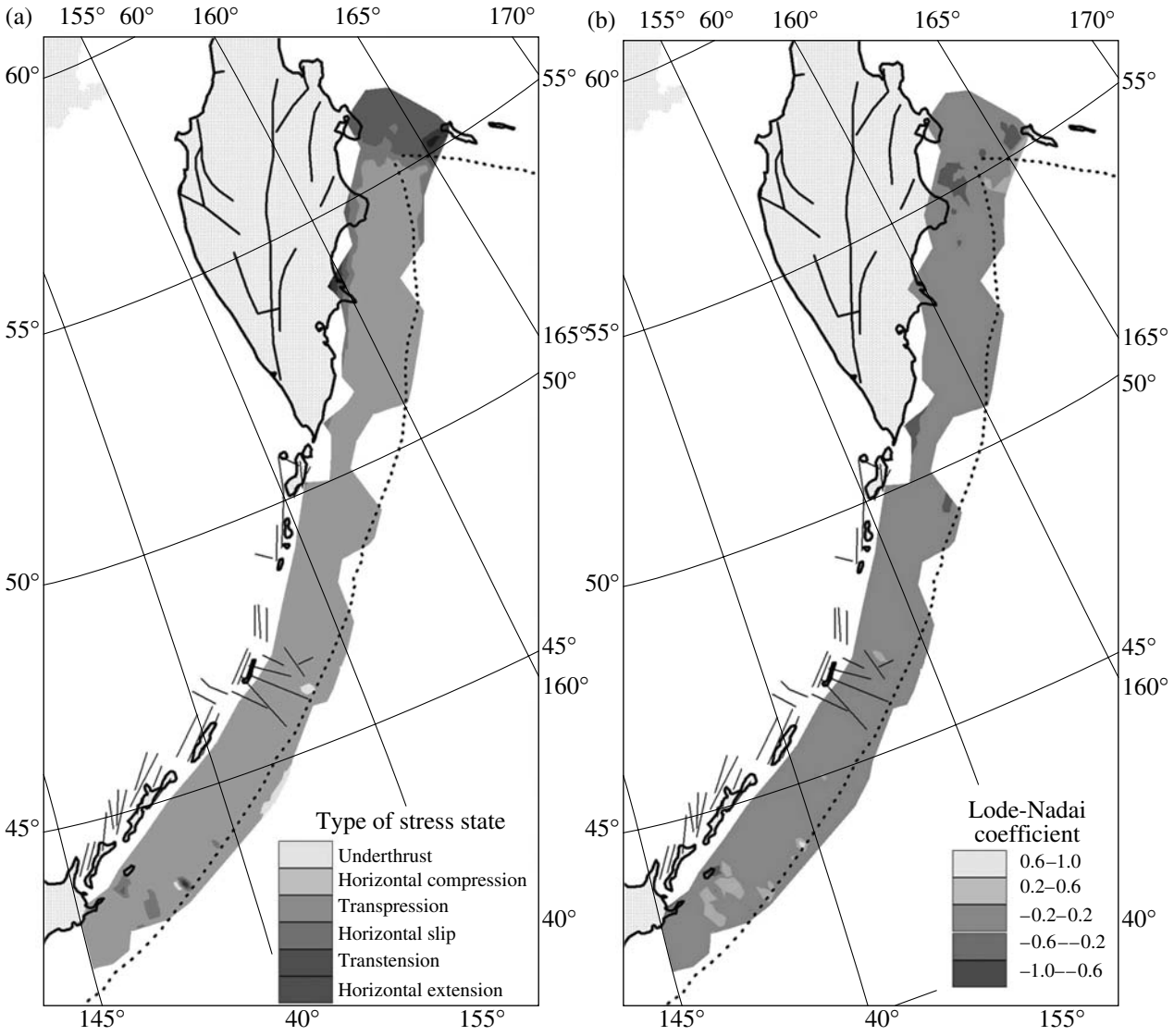

Fig. 7. Differentiation of the regions by (a) the type of stress state and (b) the type of stress tensor defined by the Lode–Nadai coefficient.

ure (the field between the outer envelope and the line of the static friction).

The source zone of the analyzed earthquake extends for approximately 240 km along the trench and includes 145 domains for which the components of the stress tensor were obtained (Figs. 5, 7, 10). These domains cover ~85% of the source zone. Since the absence of stress data is usually related to the absence of earthquake focal mechanism data, it can be supposed that not only the limiting state (the contact of the failure envelope with the large Mohr circle; Fig. 1) but also the state of activation of preexisting fractures (the large Mohr circle does not intersect the line of the minimum dry friction; Fig. 1) were not attained in these areas. In accordance with Eq. (4), the normalized values of the relaxed stresses, $\Delta\tau_n/\tau_f$, can be calculated for these domains. Note also that there are domains in Fig. 12b with negative $\Delta\tau_n/\tau_f$ values (denoted by circles). They are confined to the upper boundary of the source parallel to the trench axis. The destruction of these domains was accompanied by the influx of energy into the rock mass rather than the release of elastic energy. This situation is explained by the difference between the direction of the vector of the average displacement at the source and the direction of the vector of the shear stresses for these domains on the rupture plane (the angle between the vectors is higher than 90°) [15].

Using the parameters of the stress state of these domains and summing the contribution to the relaxed stresses for the source area within each of the domains, we obtain from Eq. (4) $\Delta\tau_n/\tau_f = 1.42$. Then, using the value of the relaxed stresses previously obtained from the seismological data, the effective cohesion can be obtained as $\tau_f = 12 \times 10^5$ Pa. The calculated τ_f value is

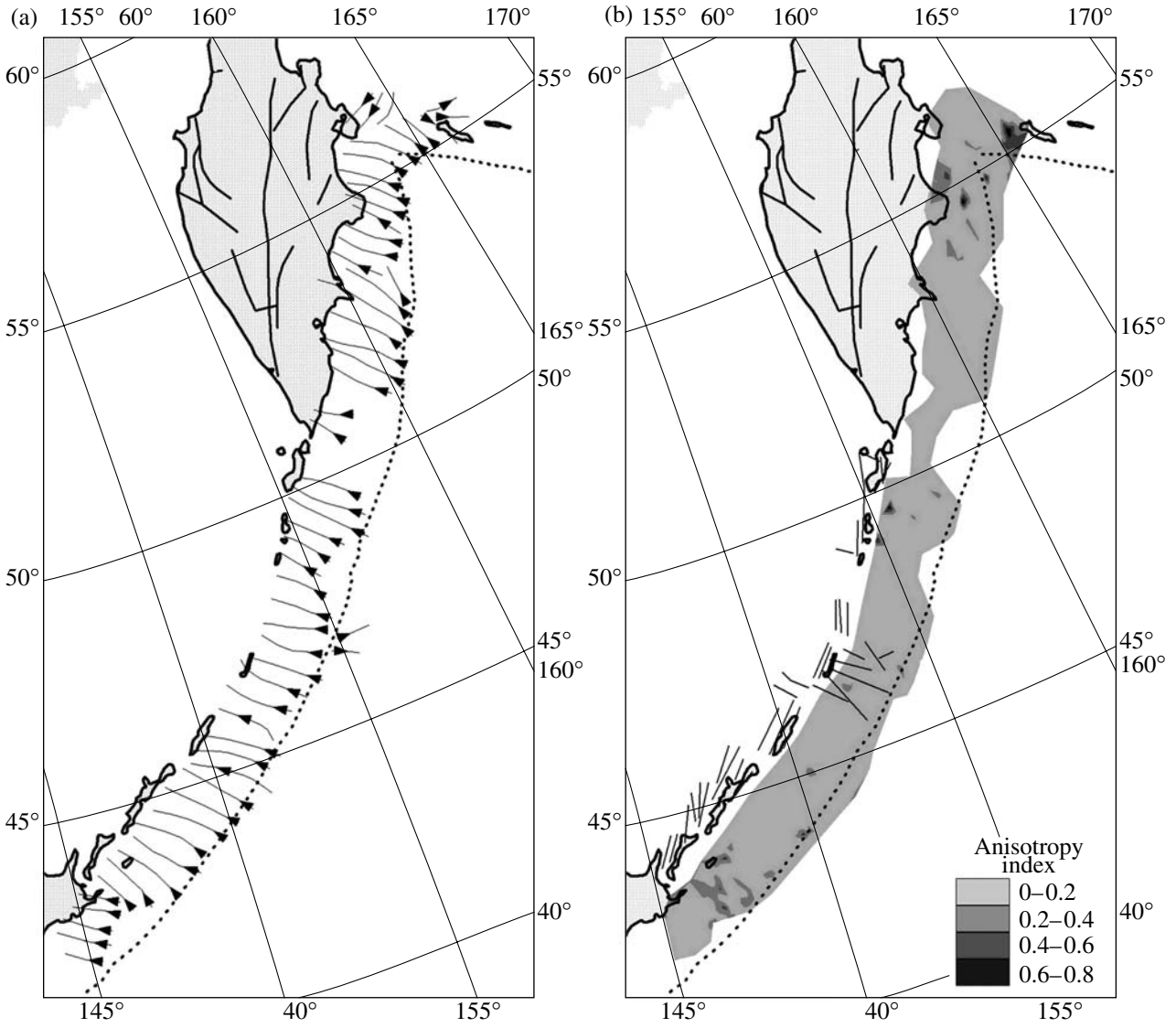

Fig. 8. (a) Direction of the underthrust shear stresses and (b) the differentiation of the regions with respect to the degree of similarity of the ellipsoids of the stresses and seismotectonic strain increments.

one and a half orders of magnitude lower than the experimental values of the cohesion obtained for small samples (a few centimeters) of the crystalline rocks. It is also lower than the value (35×10^5 Pa) obtained for the western flank of the Sunda subduction zone on the basis of the energy parameters of the Sumatra–Andaman earthquake of December 26, 2006. However, during the MCA calculations of the normalized relaxed stresses for the Sumatra–Andaman earthquake, only 30% of its source zone was covered with domains whose stress parameters were known, and this fact decreases the accuracy of the determination of the strength parameters.

Given the τ_f value, the absolute values of the effective stresses can be determined. Figure 13 shows the distribution of the maximum shear stresses and the underthrust shear stresses acting on the horizontal planes in the crust of the region. Similar to the effective confining pressure (Fig. 10a), there are quasi-homogeneous areas and areas with mosaic alternation of higher and lower values of this parameter. In accordance with Fig. 11, the domains with high τ values are characterized by high p^* values.

In the southwestern flank of the seismically active region considered, the distribution of the shear stresses acting on the horizontal planes is similar to the distribution of τ. However, in the central part and the northeastern flank of this region, the difference in the distribution of these parameters is significant. The areas of high τ_z values can be interpreted as lock zones through which the mantle influences the crust, and the areas of low values are the zones where the mantle–crust contact is dis-

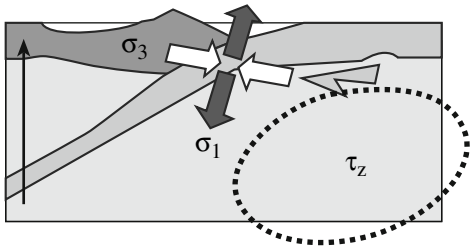

Fig. 9. Schematic diagram showing the orientation of the axes of the principal stresses and the maximum shear stresses in a subducted lithospheric plate corresponding to the convection mechanism of loading.

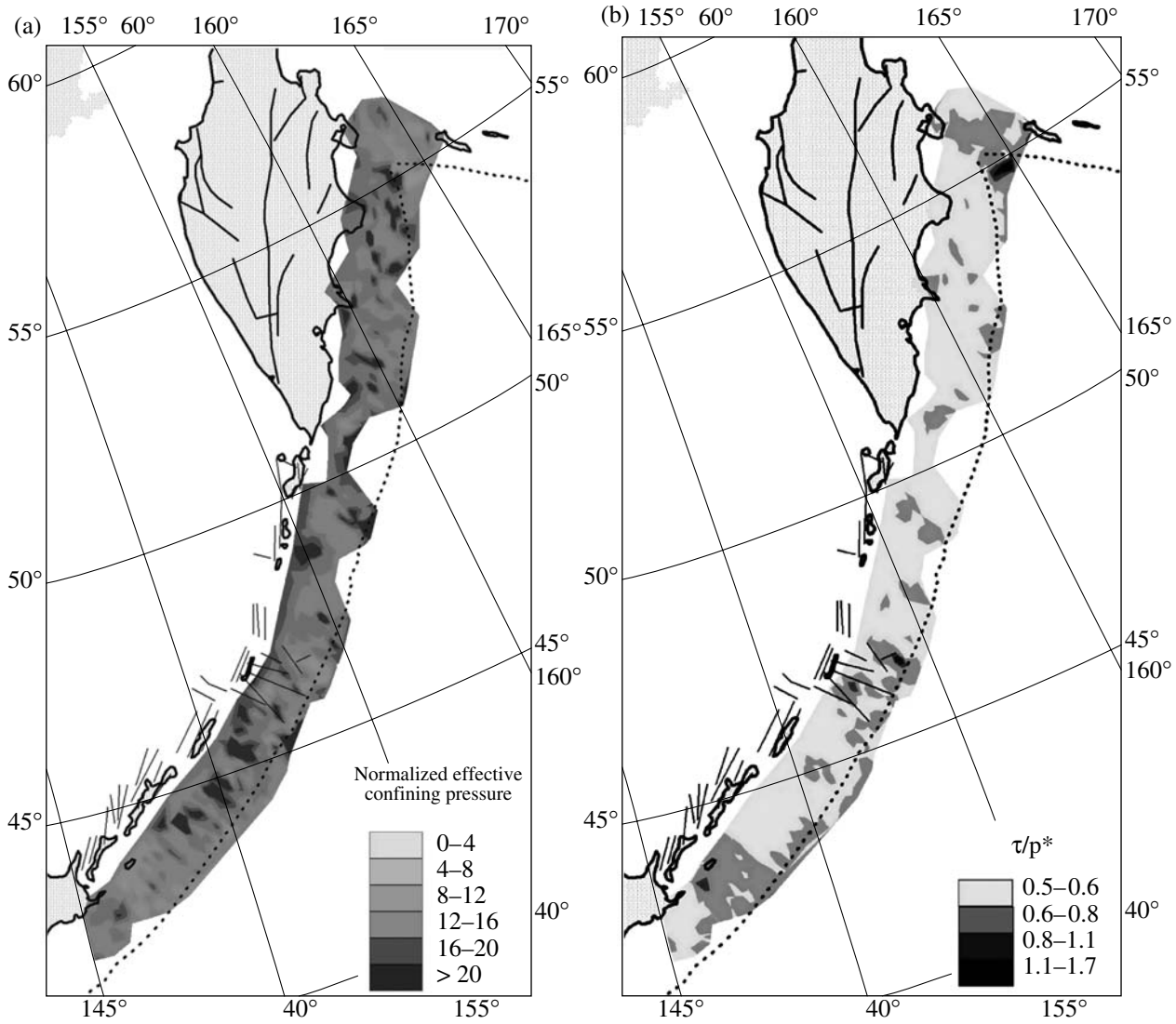

Fig. 10. Distribution of (a) the normalized effective confining pressure and (b) the maximum shear stress.

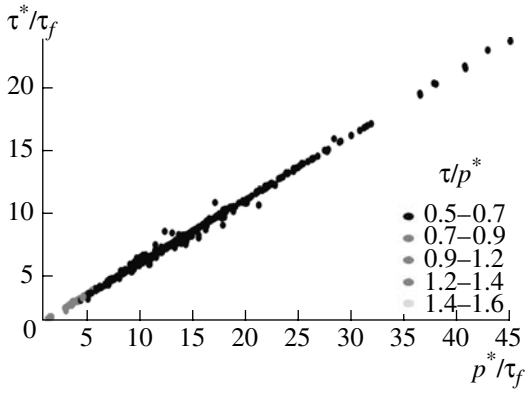

Fig. 11. Correlation of the normalized effective confining pressure p^*/τ_f with the maximum shear stress τ/τ_f. The variations in the τ/p^* ratio are shown by different shades of gray color.

turbed. The onset of the ripping of the Simushir earthquake corresponded to the zone of the minimum values of these stresses.

Fourth Stage of the Stress Reconstruction

Using Eq. (7) and the data on land and ocean floor topography, the pressure in the solid framework of rocks, p, can be calculated. Figure 14a shows the distribution of the ratio of the confining pressure to the lithostatic pressure $p_{lt} = \gamma h$ (h is the depth of the center of the domain). The p/p_{lt} value ranges from 0.985 to 1.057 and averages 1.012. The deviation of the average value from the lithostatic pressure (0.012) is about 17% of the range of its variations (0.072), which is significantly higher than the corresponding parameter for the crust of the Altai and Sayan (~1.5%) reported in [13]. The deviation of these parameters characterizes the magnitude of the external (lateral relative to the region studied) pressure superimposed upon the stress variations related to the internal heterogeneities. This and the analysis of the shear stresses on horizontal planes indicate that the contribution of the external (relative to the region) influences to the stress state probably accounts for 70–80% of the level of the deviatoric stresses produced by the weight of the rocks and seawater.

Figure 14b shows the correlation of p/p_{lt} with the maximum shear stress values and the relative fluid pressure in the fracture–pore space, p_{fl}/p_{lt}, observed in the domains for which the stress parameters were calculated. The fluid pressure was calculated from the effective confining pressure and the pressure in the rock framework, $p_{fl} = p - p^*$. The diagram allows us to suppose a quasi-linear relation between τ and p/p_{lt}. An increase in p/p_{lt} is accompanied by an increase in the shear stresses. In the domains with similar p/p_{lt} levels, an increase in the fluid pressure results in a decrease in the shear stresses.

CONCLUSIONS

The analysis of the character of the stress state in the preparation zone of the Simushir earthquake of November 15, 2006, did not reveal areas with high underthrust shear stresses. Such areas reflect the degree of the influence of the mantle on the crust (Fig. 13b). They could have corresponded to the zones where the crust exerts an especially strong resistance to displacements induced by mantle flows. The absence of such areas indicates the relatively uniform distribution of the friction forces in the lower crust. This region is almost free

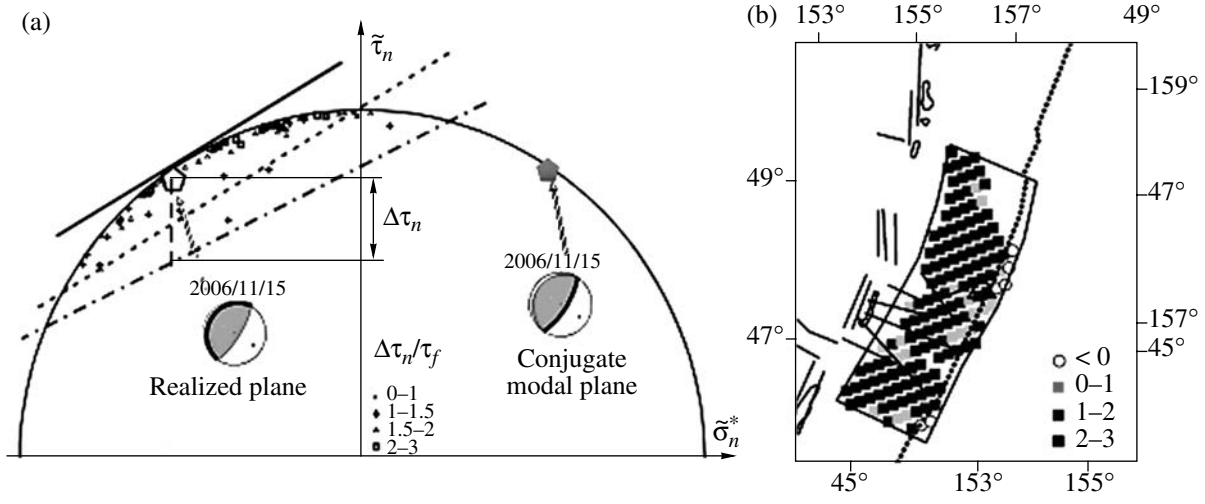

Fig. 12. The parameters of the source of the Simushir earthquake of November 15, 2006.
(a) Selection within the MCA of one of two nodal planes (the thickened semicircle in the diagram of the focal mechanism) as an active rupture using the reduced Mohr diagram (the tangent to the large Mohr circle is the strength limit, the dashed line is the minimum dry static friction, and the dash-and-dot line is the dry kinematic friction), see also Fig. 3. (b) Distribution of the normalized values of the relaxed stresses $\Delta\tau_n/\tau_f$ within the earthquake source (rectangular area).

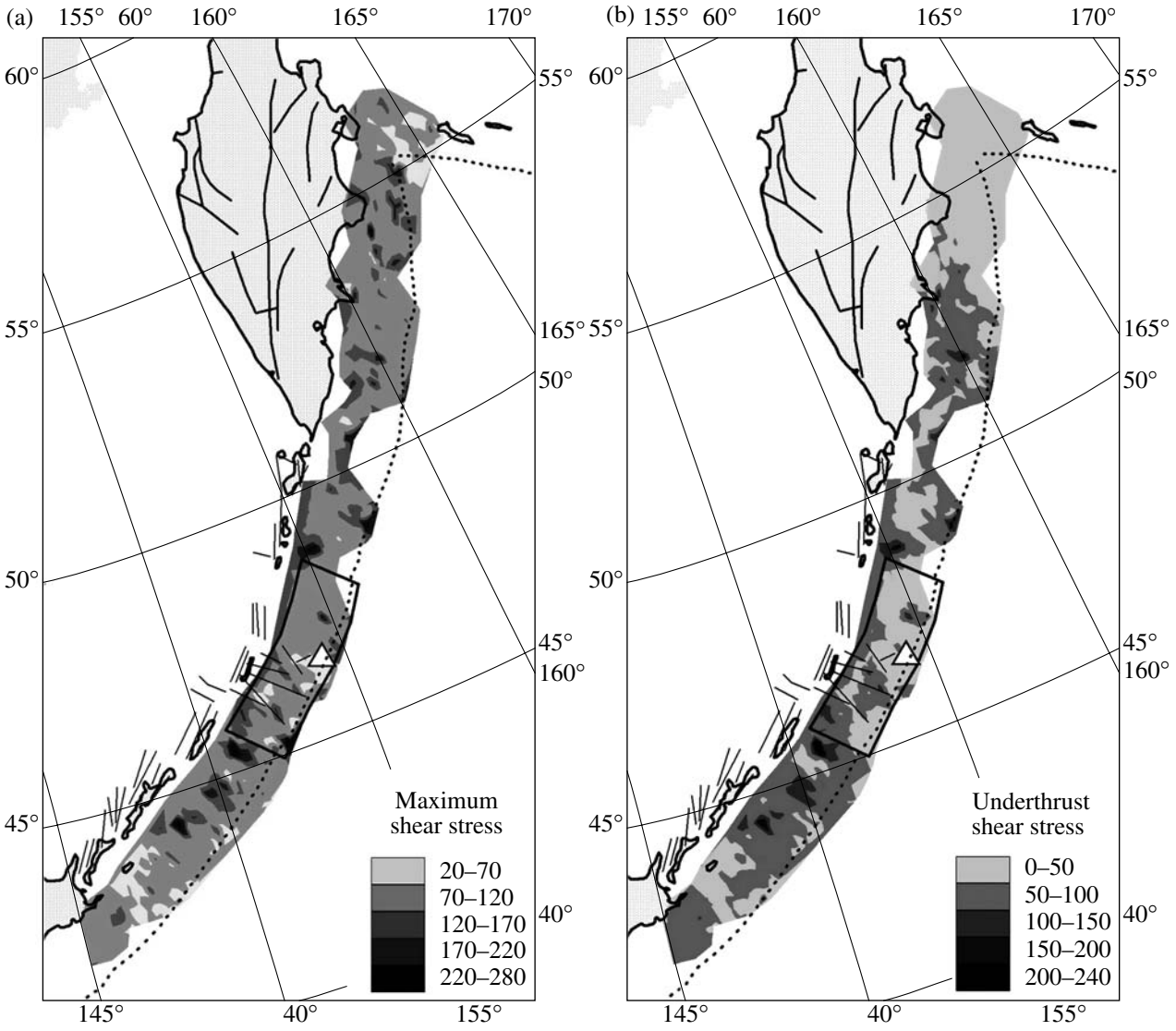

Fig. 13. Distribution of (a) the maximum shear stresses (τ, $\times 10^5$ Pa) and (b) underthrust shear stresses (τ_z) acting on the horizontal plane.

of local areas (mosaics) with elevated levels of effective confining pressure (Fig. 10a). Such areas are confined to the boundaries of this zone. The same is true for the distribution of the maximum shear stresses (Fig. 13a), because these two characteristics are interrelated (Fig. 11). Note also that the onset of ripping was confined to the boundary of the segment with the minimum values of the effective confining pressure, where the maximum gradient of this parameter was observed. These observations are in good agreement with the concept developed by us [11, 14] concerning distinguishing the areas with high seismic potentials.

According to this concept, the high efficiency of brittle failure is observed in the areas with medium levels of deviatoric and isotropic stresses. The maximum of the relaxed stresses is observed there (Fig. 1). In the areas of elevated stress levels, the plastic or cataclastic (numerous weak events) flows are more efficient. The size of the area with medium stress levels defines the magnitude of the expected event. The realization of destruction in such an area requires that the incipient rupture should overcome the resistance of those zones where brittle failure is less efficient (local islands with elevated levels of isotropic stresses and elevated friction forces). Because of this, on the one hand, it is important that this area is sufficiently homogenous with respect to the stress level, and, on the other hand, a high initial energy pulse is needed at the site of the rupture generation. Such a situation appears in areas with an elevated stress gradient. The propagation of destruction in such areas from the zone of high stresses to the zone

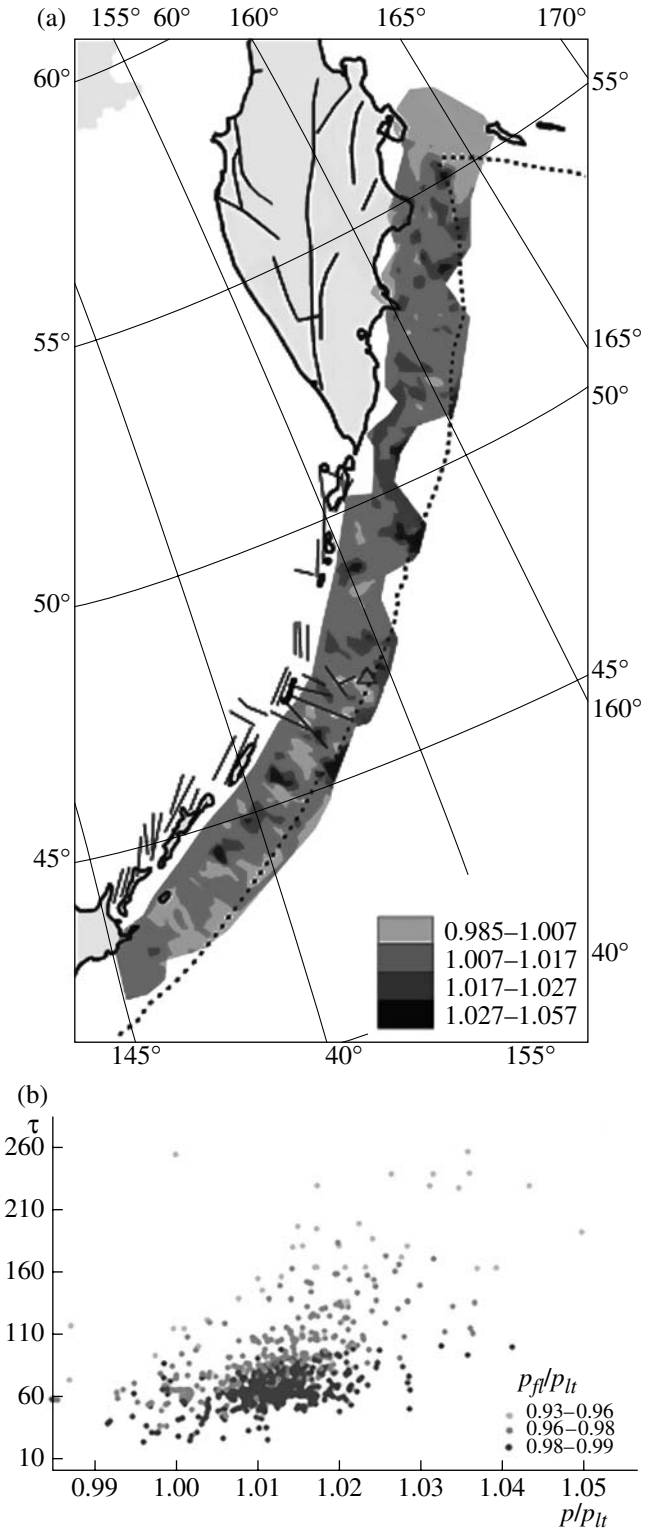

Fig. 14. (a) Distribution of the normalized value of the tectonic pressure p/p_{lt} and (b) the correlation of p/p_{lt} with the maximum shear stress (τ, $\times 10^5$ Pa) and the normalized value of the fluid pressure p_{fl}/p_{lt}. The different shades of gray filling correspond to the different values of the normalized fluid pressure p_{fl}/p_{lt}.

of low stresses is accompanied by an increase in the release of elastic strain energy.

ACKNOWLEDGMENTS

This study was financially supported by the Russian Foundation for Basic Research (project nos. 06-05-64410 and 07-05-64998) and the Department of Earth Sciences of the Russian Academy of Sciences (program no. 6).

REFERENCES

1. M. V. Gzovskii, *Principles of Tectonophysics* (Nauka, Moscow, 1975) [in Russian].
2. S. V. Gol'din, "Dilatancy, Repacking, and Earthquakes," Fiz. Zemli, No. 10, 37–54 (2004).
3. O. I. Gushchenko, "Seismotectonic Stress Monitoring of the Lithosphere: The Structural Kinematic Principle and Basic Features of the Algorithm," Dokl. Akad. Nauk **346** (3), 399–402 (1996) [Dokl. Earth Sci. **346**, 144–147 (1996)].
4. A. A. Dobrynina, "Rates and Direction of Faults in Sources of the 1999 South Baikal Earthquake Successions," in *Proceedings of the 9th Uralian Youth Scientific School on Geophysics. Modern Problems of Geophysics, Yekaterinburg, Russia, 2008* (Izd. Inst. Geol. Fiz. Ural. Otd. Ross. Akad. Nauk, Yekaterinburg, 2008), pp. 55–57 [in Russian].
5. B. V. Kostrov, *Mechanics of Tectonic Earthquake Source* (Nauka, Moscow, 1975) [in Russian].
6. Yu. L. Rebetsky, "Reconstruction of Tectonic Stress and Seismotectonic Strains: Methodical Fundamentals, Current Stresses Field of Southeastern Asia and Oceania," Dokl. Akad. Nauk **354** (1), 101–104 (1997) [Dokl. Earth Sci. **354** (4), 560–563 (1997)].
7. Yu. L. Rebetsky, "Methods for Reconstructing of Tectonic Stresses and Seismotectonic Deformations Based on the Modern Theory of Plasticity," Dokl. Akad. Nauk **365** (3), 392–395 (1999) [Dokl. Earth Sci. **365A** (3), 370–373 (1999)].
8. Yu. L. Rebetsky, "Principles of Stress Monitoring and Method of Cataclastic Analyses of Shear Totalities," Byul. Mosk. O-va Ispyt. Prir., Ser. Geol. **76** (4), 28–35 (2001).
9. Yu. L. Rebetsky, "Development of the Method of Cataclastic Analysis of Shear Fractures for Tectonic Stresses Estimation," Dokl. Akad. Nauk **388** (2), 237–241 (2003) [Dokl. Earth Sci. **388** (1), 72–76 (2003)].
10. Yu. L. Rebetsky, "Estimation of Relative Stress Values: Second Stage of Reconstruction from Data on Fault Displacements," Geofiz. Zh. Kiev **27** (1), 39–54 (2005) [in Russian].
11. Yu. L. Rebetsky and A. V. Marinin, "Field of Tectonic Stresses before the December 26, 2004 Sumatra–Andaman Earthquake. Model of Metastable State of Rocks," Geol. Geofiz. **47** (11), 1192–1206 [in Russian].
12. Yu. L. Rebetsky and A. V. Marinin, "Stressed State of the Earth's Crust in the Western Region of the Sunda Subduction Zone before the Sumatra–Andaman Earthquake on December 26, 2004," Dokl. Akad. Nauk **407** (1), 106–

109 (2006–2) [Dokl. Earth Sci. **407** (2), 321–325 (2006–2)].

13. Yu. L. Rebetsky, O. A. Kuchai, and A. V. Marinin, "Stressed State of the Earth's Crust in Altai and Sayan before 2003 Chuya Earthquakes," in *Proceedings of All-Russian Conference with International Participation on Problems of Modern Seismology and Geodynamics of Central Asia, Irkutsk, Russia, 2007* (Izd. Inst. Zem. Kory Sib. Otd. Ross. Akad. Nauk, Irkutsk, 2007), pp. 106–111 [in Russian].
14. Yu. L. Rebetsky, "New Data on Natural Stresses in Area of Preparation of Strong Earthquakes. Model of Earthquake Focal Zones," Geofiz. Zh. **29** (6), 92–110 (2007).
15. Yu. L. Rebetsky, *Tectonic Stresses and Strength of Mountain Massifs* (Nauka, Moscow, 2007) [in Russian].
16. K. Tertsagi, *Theory of Soil Mechanics* (Gosstroiizdat, Moscow, 1961) [in Russian].
17. S. A. Fedotov, "Seismic Cycles, Possibility of Quantitative Zoning and Long-Term Seismic Forecast," in *Seismic Zoning of the USSR* (Nauka, Moscow, 1968), pp. 121–130 [in Russian].
18. S. L. Yunga, *Methods and Results of Studying Seismotectonic Deformations* (Nauka, Moscow, 1990) [in Russian].
19. J. Angelier, "From Orientation to Magnitude in Paleostress Determinations Using Fault Slip Data," J. Struct. Geol. **11** (1/2), 37–49 (1989).
20. J. D. Byerlee, "Friction of Rocks," Pure Appl. Geophys. **116**, 615–626 (1978).
21. E. Carey-Gailhardis and J. L. Mercier, "A Numerical Method for Determining the State of Stress Using Focal Mechanisms of Earthquake Populations: Application to Tibetan Teleseismic and Microseismicity of Southern Peru," Earth Planet. Sci. Let. **82**, 165–179 (1987).
22. J. W. Gephart and D. W. Forsyth, "An Improved Method for Determining the Regional Stress Tensor Using Earthquake Focal Mechanism Data: Application to the San Fernando Earthquake Sequence," J. Geophys. Res. **89** (B11), 9305–9320 (1984).
23. http://earthquake.usgs.gov/eqcenter/eqachives/poster/2006/20061115_image.php.
24. http://www.globalcmt.org.
25. Yu. L. Rebetsky, "I. Stress-Monitoring: Issues of Reconstruction Methods of Tectonic Stresses and Seismotectonic Deformations," J. Earthq. Pred. Res. Beijing, China **5** (4), 557–573 (1996).
26. Yu. L. Rebetsky, A. V. Mikhailova, G. V. Rosanova, and E. V. Fursova, "II. Stress-Monitoring: The Modern Field of Regional Stresses in South East Asia and Oceania. Principles of Quasiplastic Deforming of Fractured Media," J. Earthq. Pred. Res. Beijing, China **6** (1), 11–36 (1997).
27. R. H. Sibson, "Frictional Constraints on Thrust, Wrench and Normal Faults," Nature **249** (5457), 542–544 (1974).